Small-Volume Microstrip Patch Antennas Exactly Covering Wi-Fi 6 Bands of 2.4–2.5 GHz and 5.15–5.85 GHz

Shan Gao, *Student Member, IEEE*, Le Chang, *Senior Member, IEEE*, Anxue Zhang, Yue Li, *Senior Member, IEEE*, and Zhijun Zhang, *Fellow, IEEE*

***Abstract*— The sixth generation of wireless fidelity (Wi-Fi 6) spectrums possess two unbalanced bands of 2.4–2.5 GHz (4.1%) and 5.15–5.85 GHz (12.7%). Most of the existing dual-band Wi-Fi 6 patch antennas are with either a superfluous lower or an insufficient higher bandwidth. It remains a challenge to cover these two bands in an exact way. This article addresses the issue of the exact coverage problem of the unbalanced Wi-Fi 6 bands by engineering the $TM_{0.5,0}$ and $TM_{0.5,1}$ modes of the half-mode patch while maintaining a very small volume. The design guideline follows three steps. First, select proper patch size to make the first two modes resonate at 2.45 and 5.5 GHz using two ports. Second, optimize feeding positions to make both impedance trajectories in the Smith Chart with minimum sizes. Third, use lumped components to make the two resonances with good matching condition. Using the novel matching method, the resultant half-mode patch with a profile of 3 mm ($0.024\lambda_L/0.052\lambda_H$) and size of 22.55 × 23.95 mm^2 ($0.18 \times 0.19\lambda_L^2/0.39 \times 0.41\lambda_H^2$) exactly covers the Wi-Fi 6 bands, indicating that the antenna space is taken up fully. As far as the authors know, the proposed antenna is with the smallest volume compared to all the reported Wi-Fi 6 dual-band patch antennas. Moreover, the proposed antenna is with dual-port and aperture sharing properties, which suits the optimal Wi-Fi 6 radio frequency (RF) front-end architecture.**

***Index Terms*— Dual-band antenna, dual-port antenna, half-mode patch, microstrip patch antenna, sixth generation of wireless fidelity (Wi-Fi 6) antenna.**

I. Introduction

WIRELESS fidelity is the most important standard of the wireless local area network (WLAN) and Wi-Fi 6 is indispensable for modern mobile terminals or Internet-of-Thing (IoT) devices [1]. Wi-Fi 6 antennas, which play a significant role in wireless performance, have been studied for many years [2], [3], [4], [5], [6]. For modern 5G mobile terminals, for one thing, the newly introduced frequency bands and high MIMO specification brought by 5G make antenna numbers proliferate sharply. For another thing, the metal bezels undertake huge pressure because antennas are deployed everywhere on the metal bezels and what is even worse, the bulky battery, cameras, screens, and even speakers squeeze bezel space. Both aspects promote antenna engineers and scholars to explore new space for antennas. The terminal back cover, a space that has been neglected for decades, can provide a large area for patch antennas. Therefore, the contradiction between the increasing antenna number and decreasing bezel space intensifies the demand for small-volume patch antennas.

This work focuses on the small-volume dual-band microstrip patch antenna for the sixth generation of wireless fidelity (Wi-Fi 6) applications. The two Wi-Fi 6 bands are with the property of unbalanced frequency range: the relative bandwidth of the lower band (2.4–2.5 GHz) is 4.1%, while it is 12.7% of the higher (5.15–5.85 GHz). The relative bandwidth of higher band is approximately three times that of the lower band, resulting in an extremely unbalanced frequency range and making exact coverage of the Wi-Fi 6 bands a challenging task. "Exact" refers to that these two Wi-Fi 6 bands can be covered without any superfluous frequency range, or in other words, the −10 dB impedance bandwidths are just 2.4–2.5 GHz and 5.15–5.85 GHz exactly. If superfluous frequencies exist, it means that the antenna volume is not taken up fully and it has the potential to be miniaturized. This is undesirable for modern mobile terminals whose internal space is so precious.

We almost collected all the patch antennas operating at Wi-Fi 6 bands reported in the open literature [7], [8], [9], [10], [11], [12], [13], [14], [15], [16], [17], [18], [19], [20], [21], [22], [23], [24]. Dual-band patch can be broadly classified into two types: the first type is to construct multiple resonant structures, such as slotted patches [7], [8], multiple current paths [9], [10], [11], [12], [13], stacked patches [14], [15], [16], and parasitic patches [17], [18], [19], [20]. The second is to excite the higher order modes of rectangular and circular patches [21], [22], [23], [24]. According to the comprehensive research, most of the existing dual-band Wi-Fi 6 patch antennas cannot cover these two unbalanced bandwidths exactly and they can be divided into

Manuscript received 12 March 2023; accepted 24 April 2023. Date of publication 11 May 2023; date of current version 7 July 2023. This work was supported in part by the National Natural Science Foundation of China under Grant 62101427 and Grant U22BB2016, in part by the Key Research and Development Project of Shaanxi Province under Grant 2022GY-095, in part by the High-Level Innovation Talent Project Imported by QinChuangYuan of Shaanxi Province under Grant QCYRCXM-2022-33, and in part by the Shaanxi Key Laboratory of Deep Space Exploration Intelligent Information Technology under Grant 2021SYS-04. *(Corresponding author: Le Chang.)*

Shan Gao, Le Chang, and Anxue Zhang are with the Shaanxi Key Laboratory of Deep Space Exploration Intelligent Information Technology, School of Information and Communications Engineering, Xi'an Jiaotong University, Xi'an 710049, China (e-mail: changle4015@126.com).

Yue Li and Zhijun Zhang are with the Beijing National Research Center for Information Science and Technology, Tsinghua University, Beijing 100084, China.

Color versions of one or more figures in this article are available at https://doi.org/10.1109/TAP.2023.3273920.

Digital Object Identifier 10.1109/TAP.2023.3273920

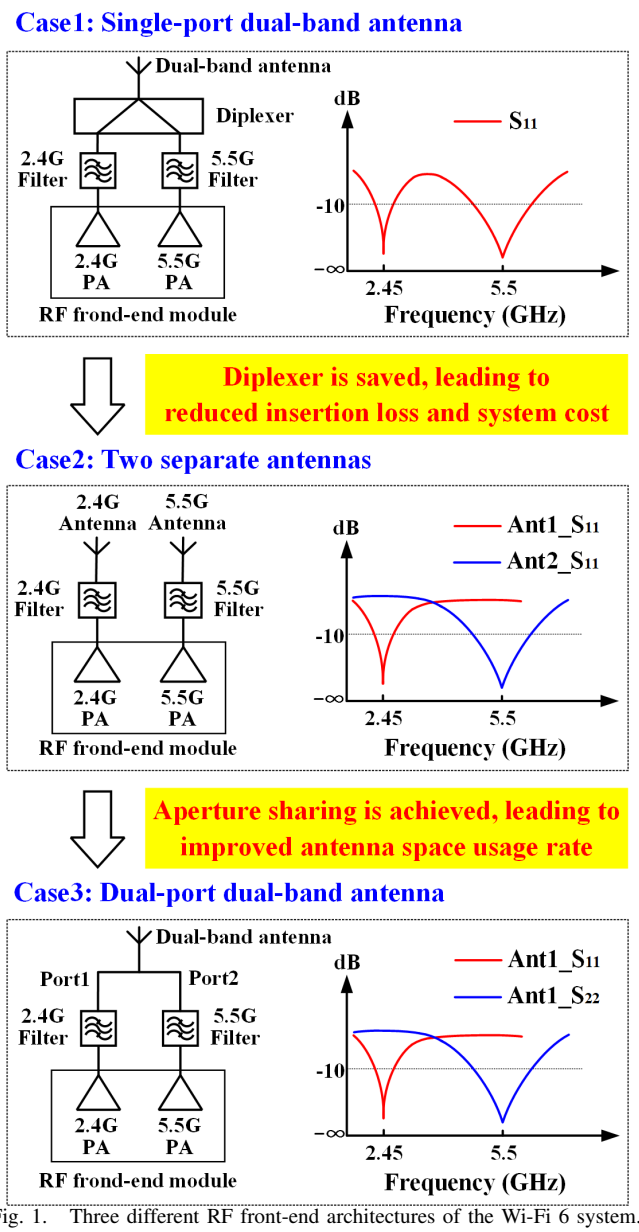

Fig. 1. Three different RF front-end architectures of the Wi-Fi 6 system.

three situations: 1) the Wi-Fi 6 lower band can be covered, whereas the higher cannot, e.g., antennas in [7], [11], [16], [21], and [23] suffer from insufficient higher band coverage: their bandwidths are 5.14–5.39 GHz, 5.55–5.97 GHz, 5.72–5.88 GHz, 4.72–5.36 GHz, and 5.42–5.98 GHz; 2) the higher band can be covered, but the lower is superfluous, e.g., antennas in [10] and [14] suffer from superfluous lower band coverage: their bandwidths are 2.28–2.55 GHz and 2.4–2.65 GHz, which means that the antenna volumes are not taken up fully; 3) both lower and higher bands cannot be covered totally, such as antennas in [8], [12], [13], and [24] with the bandwidths of 2.39–2.42 GHz/4.94–5.07 GHz, 2.44–2.45 GHz/5.53–5.88 GHz, 2.4–2.48 GHz/5.73–5.88 GHz, and 2.36–2.44 GHz/5.7–5.9 GHz. Therefore, it is a great challenge to cover the unbalanced Wi-Fi 6 bands in an exact way. Moreover, small-volume property is the permanent pursuit for mobile terminal antennas.

Traditionally, when an antenna needs to be matched, for antenna with natural resonance electrical size, such as normal/half-mode patch with length of half/quarter wavelength, it usually selects the feeding position where the electric divided by magnetic equals 50 Ω. This is called the traditional matching method and the resultant operating frequency is natural resonance. For small-sized electrical antennas, such as half-mode patch with a length smaller than a quarter wavelength, lumped components are used to make the target frequency resonant with 50-Ω input impedance [25]. This is called component matching method. In this article, we neither use traditional nor component matching method but combine these two to achieve improved antenna performance.

Considering antenna miniaturization, half-mode patch is a good candidate compared with normal patch because its operation frequency is similar to that of normal patch, but the size is halved and quality factor (Q factor) value decreases. In this article, the first two modes of the half-mode patch excited by two separate ports are engineered for Wi-Fi 6 dual-band coverage. For a half-mode patch, different patch lengths and widths produce different natural resonances for the first two modes. For each mode, different feeding positions lead to impedance trajectories with different sizes in the Smith Chart corresponding to different Q values. The impedance trajectory with the natural resonant frequency of 2.45 GHz/5.5 GHz and with the smallest circle to enclose itself has the potential to produce the minimum Q value and the maximum impedance bandwidth for Wi-Fi 6 [26]. Therefore, the design guideline is summarized as follows: by selecting proper patch size and feeding positions, the best impedance trajectories can be achieved, and then, by resorting to the lumped components, the Wi-Fi 6 bands can be covered exactly.

The proposed antenna is with a profile of 3 mm ($0.024\lambda_L/0.052\lambda_H$) and a size of 22.55 × 23.95 mm^2 ($0.18 \times 0.19\lambda_L^2/0.39 \times 0.41\lambda_H^2$), where λ_L/λ_H refers to the lowest frequencies of the lower/higher band. The simulated result shows that the impedance bandwidths exactly cover the Wi-Fi 6 bands of 2.4–2.5 GHz and 5.15–5.85 GHz, indicating that the antenna space is taken up fully. The measured results show that the −10 dB impedance bandwidths are 5.8% (2.49–2.64 GHz) and 12.9% (5.19–5.91 GHz), the isolations at both bands are better than 32.5 dB, and the average efficiencies are −1.1 dB (77.6%) and −0.7 dB (85.1%). To the best of the authors' knowledge, the proposed antenna is with the smallest volume compared to all the reported Wi-Fi 6 dual-band patches. The properties of exact coverage and smallest volume indicate that the antenna space usage rate is extremely high. Moreover, it is with dual-port and aperture sharing properties, which suits the optimal Wi-Fi 6 radio frequency (RF) front-end architecture. The proposed antenna is suitable to be applied in modern mobile terminals or IoT devices.

II. Optimal Wi-Fi 6 RF Front-End Architecture and Small-Volume Dual-Band Wi-Fi 6 Patch Antenna

In this section, first, the Wi-Fi 6 RF front-end architectures are discussed. Second, the challenge of the exact coverage

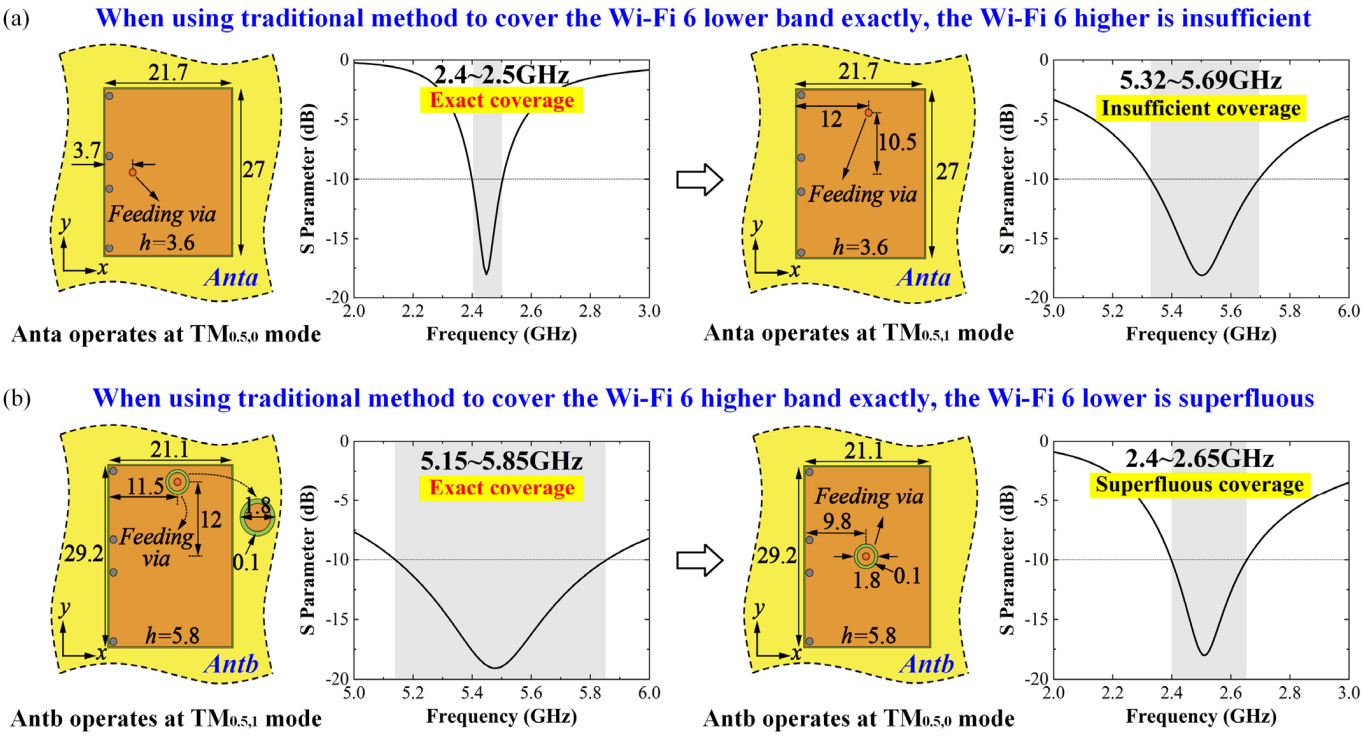

Fig. 2. Explanation of the exact coverage problem of the Wi-Fi 6 bands using the traditional matching method. (a) When the Wi-Fi 6 lower band is covered exactly, what will happen to the Wi-Fi 6 higher. (b) When the Wi-Fi 6 higher band is covered exactly, what will happen to the Wi-Fi 6 lower (unit: mm).

problem of the Wi-Fi 6 bands using the traditional method is explained. Third, the proposed antenna is introduced. Finally, the superiority of the design strategy is clarified through a comprehensive comparison.

A. RF Front-End Architecture of the Wi-Fi 6 System

The proposed antenna is not only with exact coverage and small-volume merits but also designed for the optimal Wi-Fi 6 RF front-end architecture. Fig. 1 shows three different RF front-end architectures of the Wi-Fi 6 system. The Wi-Fi 6 antenna is connected to the front-end module (FEM) after filtering. Two separated power amplifiers (PAs) of 2.4 and 5.5 GHz are included within the FEM. For Case1, the antenna is a single-port dual-band antenna and the antenna port is connected with the two output ports of the FEM through a diplexer. The drawback is that the insertion loss of the diplexer introduced deteriorates the system performance. Generally, the insertion losses are about 0.6 and 1.0 dB for these two Wi-Fi 6 bands. For Case2, 2.4- and 5.5-GHz antennas are two separate antennas and these two antenna ports are connected with the two output ports of the FEM separately without the need for a diplexer. Thus, the diplexer is saved, leading to reduced insertion loss and system cost. Case3 is with the basis of Case2. The antenna form is changed from separate aperture to shared aperture in order to save space, which is more suitable for modern mobile terminals or IoT devices. Thus, Case3 is the most advanced Wi-Fi 6 RF front-end architecture. The antenna in Case3 is a shared-aperture dual-port dual-band antenna and the proposed antenna is designed for Case3 [24].

B. Exact Coverage Problem of the Wi-Fi 6 Bands

As defined in Section I, traditional matching method refers to selecting the feeding position where the electric divided by magnetic equals 50 Ω. The exact coverage problem using the traditional matching method to cover the Wi-Fi 6 bands is explained. Fig. 2(a) and (b) shows two half-mode patches (Anta and Antb) both with the first two natural resonances resonating at 2.45 and 5.5 GHz. Fig. 2(a) shows what will happen to the Wi-Fi 6 higher when the Wi-Fi 6 lower band is covered exactly. Anta is a half-mode patch with the dimensions of 21.7 × 27 × 3.6 mm^3. When putting the feeding via at the 50-Ω impedance position of the $TM_{0.5,0}$ mode, the resultant bandwidth of 2.4–2.5 GHz covers the Wi-Fi 6 lower band exactly. When the feeding via is placed at the 50-Ω impedance position of the $TM_{0.5,1}$ mode, the resultant bandwidth is 5.32–5.69 GHz, which is insufficient for higher. Fig. 2(b) shows what will happen to the Wi-Fi 6 lower when the Wi-Fi 6 higher band is covered exactly. Antb is a half-mode patch with the dimensions of 21.1 × 29.2 × 5.8 mm^3. When putting the feeding via at the 50-Ω impedance position of the $TM_{0.5,1}$ mode, the resultant bandwidth of 5.15–5.85 GHz covers the Wi-Fi 6 higher band exactly. When the feeding via is placed at the 50-Ω impedance position of the $TM_{0.5,0}$ mode, the resultant bandwidth is 2.4–2.65 GHz, which is 2.6 times wider than the lower. The superfluous frequency range indicates that the antenna space is not taken up fully.

From the analysis above, when using the traditional matching method to produce natural resonances to cover the Wi-Fi 6 bands, either the bandwidth of the lower band will overflow or the bandwidth of higher will be too narrow, just as the first

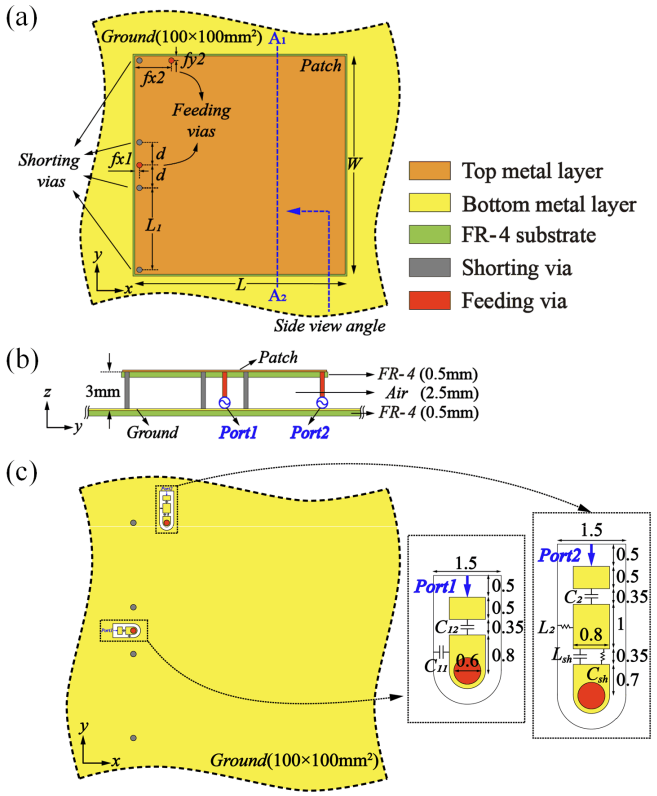

Fig. 3. Configuration of the proposed antenna. (a) Top view. (b) Side view (seen from the right of the A_1–A_2 plane). (c) Top view of the ground plane (unit: mm). Dimensions: $L = 22.55$ mm, $W = 23.95$ mm, $L_1 = 8.98$ mm, $d = 2.5$ mm, $fx1 = 0.5$ mm, $fx2 = 4$ mm, $fy2 = 0.5$ mm, $C_{11} = 1.3$ pF, $C_{12} = 1.1$ pF, $C_{sh} = 0.5$ pF, $L_{sh} = 8.7$ nH, $L_2 = 3.4$ nH, and $C_2 = 0.3$ pF.

and second situations described in Section I. It is a challenge to cover the Wi-Fi 6 bands exactly while maintaining a small volume.

C. Antenna Configuration

Fig. 3 shows the antenna configuration, which is basically a half-mode microstrip patch antenna. The whole antenna is with the dimensions of $22.55 \times 23.95 \times 3$ mm^3. The profile consists of a 0.5-mm-thick FR-4 substrate ($\varepsilon_r = 4.3$ and $\tan\delta = 0.02$) and a 2.5-mm-thick air layer, which simulates the planar back cover antenna within a realistic mobile terminal, where the top substrate is realized using a flexible printed circuit board and the middle air layer is the space between the back cover and the RF shielding case or system ground [27], [28]. A 0.5-mm-thick FR-4 substrate with its top surface plated with metal acts as the ground plane. The ground plane with the dimensions of 100×100 mm^2 is far larger than the patch, indicating that the ground does not contribute to radiation. It means that the proposed antenna is a universal strategy suitable to be implemented on various ground planes or, in other words, suitable for various mobile terminals or IoT devices [22]. If the ground plane can be customized, such as slotted ground or small ground of identical size with the patch, the antenna performance can be improved greatly [28], [29] or, in other words, the patch is able to be miniaturized further.

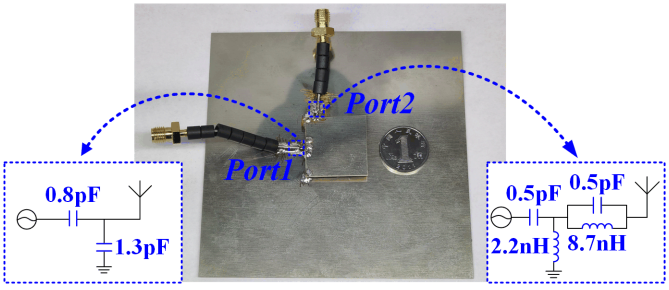

Fig. 4. Fabricated prototype.

As shown in Fig. 3(a) and (b), four shorting vias act as the shorting wall of the half-mode patch. The feeding via of port1 (lower band port) aligns with the shorting wall and locates in the middle line of the patch. These four shorting vias are distributed unevenly: the middle two vias gather together to the center of port1, which aims to make the lower bandwidth a little wider (the result is omitted because the effect is not significant). The feeding via of port2 (higher band port) locates 4 and 0.5 mm away from the left and upper patch edges, respectively. The diameters of all the vias are 0.6 mm. It is worth mentioning that the feeding positions are important for antenna bandwidths and efficiencies. Besides, the feeding positions both locate at the outside edges of the patch, which are beneficial for realistic components soldering. Frequent inductor/capacitor soldering around antenna ports is required when tuning antennas, but if the feeding positions locate totally beneath the patch, each time when changing matching components, the patch has to be removed, which greatly increases implementation complexity. The proposed antenna decouples patch implementation and impedance tuning and only needs to be assembled once.

Fig. 3(c) shows the matching topologies. For port1, two lumped components of shunt 1.3-pF capacitor cascaded by series 1.1 pF are used for impedance matching, while for port2, two lumped components of shunt 3.4-nH inductor cascaded by series 0.3-pF capacitor are used. A lumped filter composed by shunt 0.5-pF capacitor and 8.7-nH inductor is added at port2 for isolation enhancement. Each component is assigned with a 2-Ω resistor to roughly evaluate its loss in simulation. Dimensions of the solder pads can be seen in the figure.

D. Results

Fig. 4 shows the fabricated prototype. Two 50-Ω coaxial cables wrapped with magnetic beads are used to feed the patch. The practical lumped components are only slightly different from the simulation, as marked in the figure. The simulation software is the CST version 2020.

Fig. 5(a) shows the simulated and measured S-parameters and total efficiencies. The measured results agree with the simulated well. For S-parameters, the simulated -10 dB impedance bandwidths are just the Wi-Fi 6 bands, while the measured are 2.49–2.64 GHz (150 MHz, 5.8%) and 5.19–5.91 GHz (720 MHz, 12.9%). At higher band, two resonances exist, both of which operate with the same $TM_{0.5,1}$ mode and are caused by impedance matching. The results demonstrate

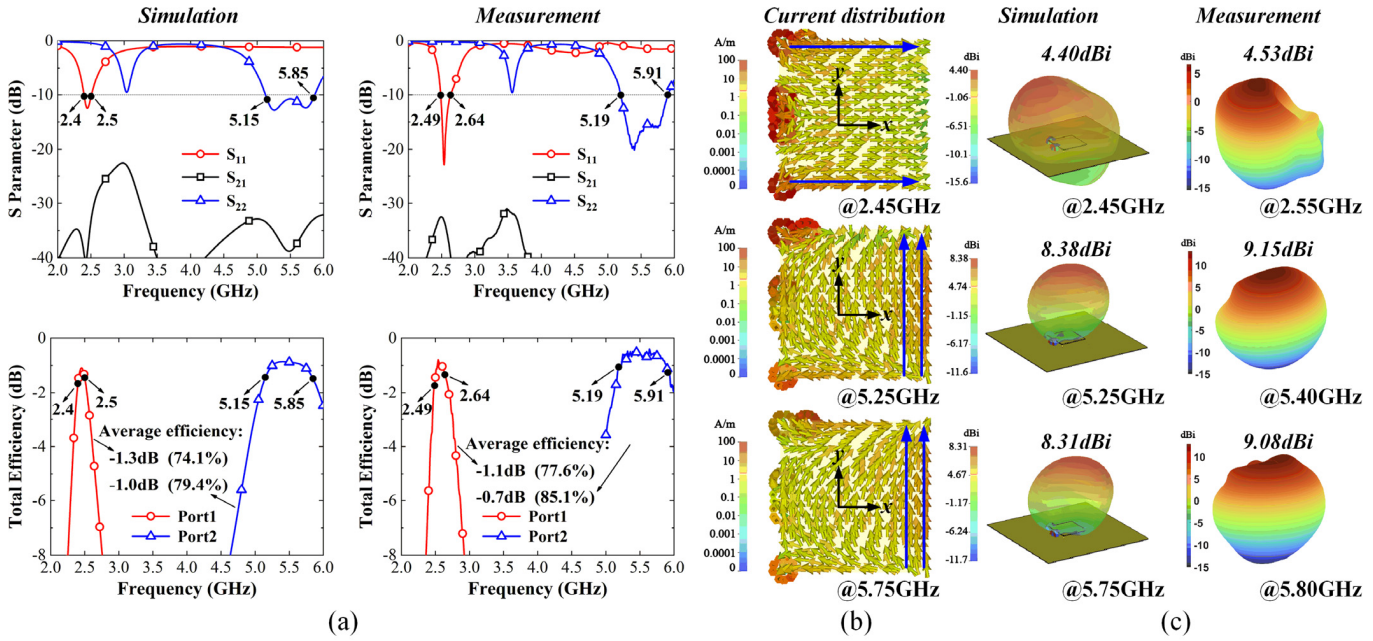

Fig. 5. (a) Simulated and measured S-parameters and total efficiencies. (b) Simulated current distributions. (c) Simulated and measured 3-D radiation patterns.

that 3 mm is the proper profile to realize the relative bandwidths of 4.1% and 12.7% at 2.45 and 5.5 GHz, respectively.

The simulated and measured isolations are better than 33.4 and 32.5 dB across the two operation bands, respectively. For average total efficiencies, the simulated results are −1.3 dB (74.1%) and −1.0 dB (79.4%) for the lower and higher bands, respectively, while the measured ones are −1.1 dB (77.6%) and −0.7 dB (85.1%). The slightly higher measured efficiencies indicate that the 2-Ω loss assumed is slightly larger. The measured high levels of isolation and efficiencies demonstrate that the proposed antenna is with excellent performance.

Fig. 5(b) shows the simulated current distributions. Classic $TM_{0.5,0}$ and $TM_{0.5,1}$ modes of the half-mode patch can be observed. The current distributions of the two resonances at higher band are the identical $TM_{0.5,1}$ mode, proving that these two resonances come from impedance matching. Fig. 5(c) shows the simulated and measured radiation patterns, which agree well. At 2.55 GHz, it is a broadside beam with the measured gain of 4.53 dBi. At 5.40 and 5.80 GHz, similar patterns both with broadside beam can be observed and the measured gains are both around 9.1 dBi.

E. Performance Comparison

To demonstrate the superiority of the design strategy, a comprehensive comparison between the proposed antenna and other dual-band Wi-Fi 6 patch antennas is shown in Table I. To compare the antenna volume and bandwidth more intuitively, the parameter, bandwidth-to-volume ratio (BVR), is introduced. BVR is defined by dividing the relative bandwidth by electrical volume, which can evaluate the usage rate of antenna volume. The references are listed in the order of antenna profile. These data are interpreted from three aspects.

First, for one thing, the proposed antenna achieves the maximum BVRs at both bands. For another thing, none of the reference antennas cover the Wi-Fi 6 dual band with an exact way, except for the proposed (the antenna in [9] almost covers the Wi-Fi 6 bands exactly, but its volume is 8.6 times larger). These two aspects prove that the proposed antenna is with the highest space usage rate.

Second, only the three antennas in [10], [9], and [14] can totally cover the Wi-Fi 6 bands, but they are all with a much higher profile and larger size. Among these three antennas, the antenna in [14] is with the lowest profile of $0.046\lambda_L/0.103\lambda_H$, which is far higher than the proposed one of $0.024\lambda_L/0.052\lambda_H$, while the antenna in [9] is with the smallest size of $0.30 \times 0.30\lambda_L^2/0.63 \times 0.63\lambda_H^2$, which is far larger than the proposed one of $0.18 \times 0.19\lambda_L^2/0.39 \times 0.41\lambda_H^2$.

Third, the proposed antenna is with significant advantage in terms of antenna size. Except for antennas in [8] and [12], others are all with a much larger electrical size at both bands. However, the bandwidths of these two antennas are too narrow to cover Wi-Fi 6: they are 1.0% and 0.6% at the lower band and 2.5% and 6.4% at the higher band.

Above all, the proposed antenna not only covers the Wi-Fi 6 bands exactly but also is with the smallest volume compared to other Wi-Fi 6 dual-band patch antennas.

III. Discussion

In this section, the proposed matching strategy is introduced in detail first. Then, the comparison between traditional and the proposed matching methods is conducted. Finally, the isolation consideration is introduced.

A. Proposed Matching Strategy

As mentioned in Section I, the patch size determines the natural resonances and the feeding positions determine the

TABLE I
PERFORMANCE COMPARISON OF THE SMALL-VOLUME DUAL-BAND PATCH ANTENNA OPERATING AT WI-FI 6 BANDS

Refs.	f_0 (GHz)	Lower Band						Higher Band						Method
		Profile (λ_L)	Size (λ_L^2)	Volume ($\lambda_L^3/10^3$)	Δf_L (%)	BVR$\times 10^3$ /λ_L^3	Gain(dBi) /Eff.(dB)	Profile (λ_H)	Size (λ_H^2)	Volume ($\lambda_H^3/10^3$)	Δf_H (%)	BVR$\times 10^3$ /λ_H^3	Gain(dBi) /Eff.(dB)	
[10]	2.40~2.65 Sup 5.00~6.40 Sup	0.128	0.30×0.30	11.5	9.9	0.86	7.85/-	0.267	0.63×0.63	105.97	24.6	0.23	9.7/-	Multiple paths
[9]	2.40~2.50 Exa 5.10~5.90 Exa	0.096	0.34×0.21	6.85	4.1	0.60	7.5/-	0.200	0.72×0.43	61.92	18.2	0.29	9.5/-	Multiple paths
[21]	2.36~2.54 Sup 4.72~5.36 Ins	0.071	0.31×0.51	11.23	7.3	0.65	7.2/-	0.142	0.53×0.72	54.19	12.7	0.23	8.5/-	Higher-order mode
[11]	2.37~2.49 Exa 5.55~5.97 Ins	0.052	0.32×0.26	4.33	4.9	1.13	9.6/-0.5	0.12	0.74×0.60	53.28	7.3	0.14	10.2/-1.0	Multiple paths
[14]	2.28~2.55 Sup 5.15~5.90 Exa	0.046	0.72×0.72	23.85	11.2	0.47	-	0.103	1.62×1.62	270.31	13.6	0.05	6.0/-	Stacked patch
[8]	2.39~2.42 Ins 4.94~5.07 Ins	0.039	0.10×0.10	0.39	1.0	2.56	3.3/-	0.081	0.21×0.21	3.57	2.5	0.70	5.5/-	Slotted patch
[23]	2.24~2.53 Sup 5.42~5.98 Ins	0.031	0.69×0.69	14.76	12.1	0.82	6.0/-0.46	0.075	1.66×1.66	206.67	9.8	0.05	7.5/-1.0	Higher-order mode
[16]	2.40~2.50 Exa 5.72~5.88 Ins	0.026	0.24×0.36	2.25	4.1	1.82	3.1/-	0.061	0.57×0.86	29.90	2.8	0.09	0.6/-	Stacked patch
[19]	2.40~2.44 Ins 5.10~6.00 Sup	0.024	0.80×0.64	12.29	1.7	0.14	5.1/-2.0	0.051	1.70×1.36	120.22	16.2	0.13	6.3/-1.5	Parasitic patch
[12]	2.44~2.45 Ins 5.53~5.88 Ins	0.016	0.20×0.18	0.58	0.6	1.03	5.0/-	0.037	0.44×0.40	6.51	6.4	0.98	7.6/-	Multiple paths
[7]	2.40~2.50 Exa 5.14~5.39 Ins	0.014	0.29×0.28	1.14	4.1	3.60	2.3/-	0.029	0.61×0.60	10.61	4.7	0.44	3.6/-	Slotted patch
[24]	2.36~2.44 Ins 5.70~5.90 Ins	0.012	0.55×0.55	3.63	3.5	0.96	1.7/-	0.030	1.33×1.33	53.07	3.4	0.06	6.8/-	Higher-order mode
[13]	2.40~2.48 Ins 5.73~5.88 Ins	0.008	0.53×0.17	0.72	3.4	4.72	4.0/-4.0	0.019	1.26×0.40	9.58	2.6	0.27	5.5/-1.2	Multiple paths
Pro.	**2.40~2.50 Exa** **5.15~5.85 Exa**	**0.024**	**0.18×0.19**	**0.82**	**4.1**	**5.00**	**4.4/-1.3**	**0.052**	**0.39×0.41**	**8.31**	**12.7**	**1.53**	**8.35/-1.0**	**Novel matching strategy**

*Only simulated results are provided.
*Sup, Ins, and Exa refer to superfluous, insufficient, and exact coverage, respectively.

size of the impedance trajectories. The impedance trajectory with the natural resonance at the target center frequency and with the smallest size has the potential to produce the maximum impedance bandwidth. In this section, the proposed matching strategy aiming to achieve the maximum impedance bandwidths and address the exact coverage problem is introduced in detail. As shown in Fig. 6, the initial S_{11}, final S_{11}, final total efficiency, and initial/final impedance trajectories in the Smith Chart are presented to explain the design process.

Fig. 6(a) and (b) shows the influence of the patch length and port1's position, respectively. When the length increases from 20.55 to 22.55 to 24.55 mm, the initial S_{11} exhibits a natural characteristic center frequency of 2.30, 2.45, and 2.63 GHz. When the lumped components are loaded to make patches with different lengths resonate at 2.45 GHz, the final S_{11} and total efficiency show that the patch with the natural frequency just at 2.45 GHz achieves the minimum Q factor, maximum bandwidth, and best efficiency. The cases of 20.55 and 24.55 mm may obtain the maximum bandwidths at their own natural frequencies. Thus, the patch length is selected to make the initial natural characteristic center frequency of the $TM_{0.5,0}$ mode resonate at 2.45 GHz. As shown in Fig. 6(b), when port1's position moves from the open to the shorting edge (*fx1* decreases from 22.5 to 11.5 to 0.5 mm), as seen from the rightmost Smith Chart figure, the impedance trajectory gradually shrinks and Q value reduces, so the resultant bandwidth gradually widens and total efficiency gets better. Thus, port1's position is selected to be aligned with the shorting edge. When the best patch length and port1's position are selected, not only the impedance bandwidth of the $TM_{0.5,0}$ mode reaches the maximum, but also the Wi-Fi 6 lower band can be covered exactly. It is worth mentioning that the performance at the lower band is slightly affected by the feeding position, whereas

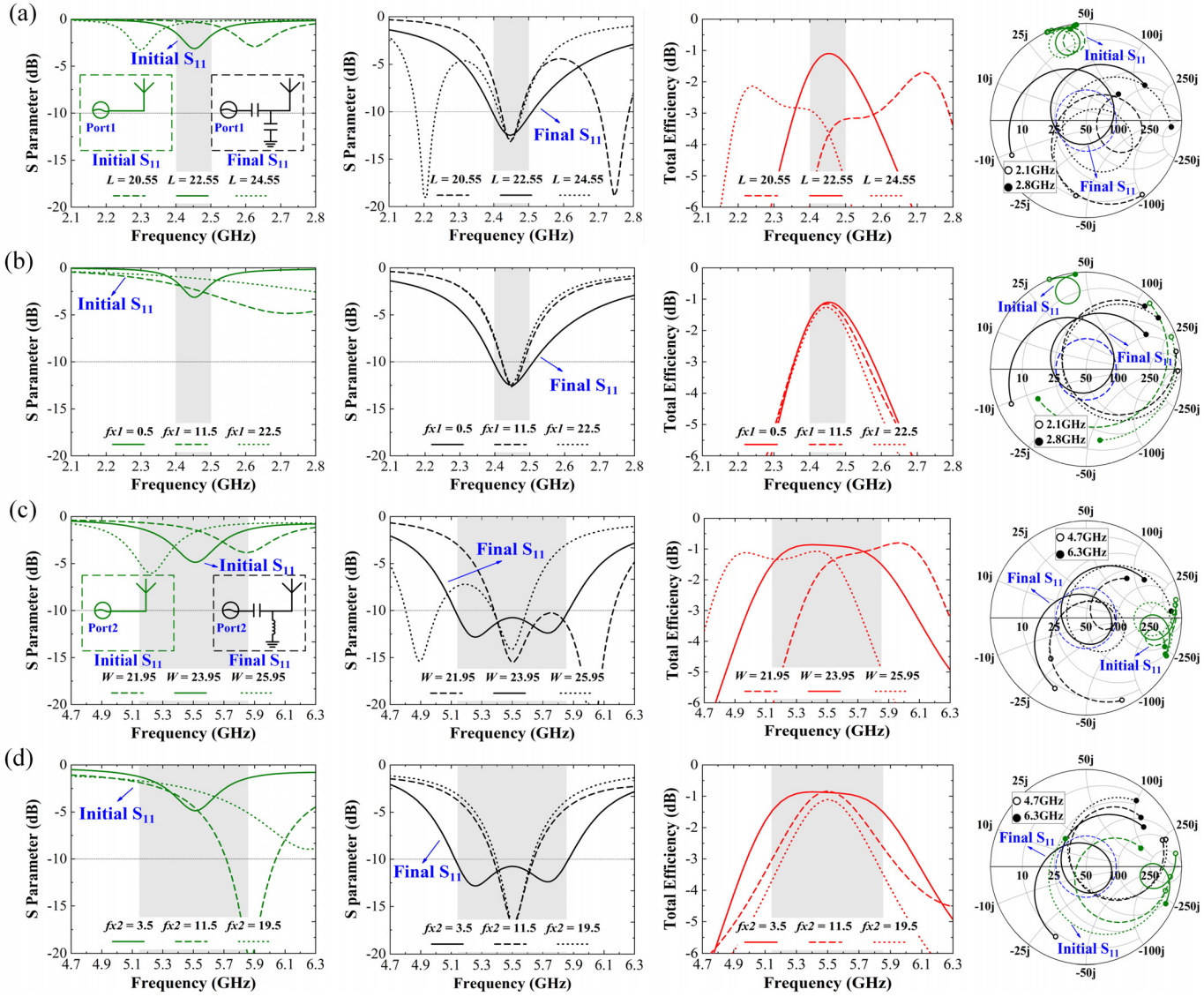

Fig. 6. Proposed matching strategy explanation. Simulated S-parameters and total efficiencies of the proposed antenna for different (a) patch lengths, (b) port1's positions, (c) patch widths, and (d) port2's positions (unit: mm).

the performance at the higher band is significant, as shown in the following.

Fig. 6(c) and (d) shows the influence of the patch width and port2's position, respectively. The analysis process is just the same as the case of the lower band. As seen from Fig. 6(a) and (c), the influence of the patch width on higher band is as significant as that of patch length on the lower band. As seen from Fig. 6(b) and (d), the influence of port2's position on the higher band is much greater than on the lower band. The patch width is selected to make the initial natural characteristic center frequency of the $TM_{0.5,1}$ mode resonate at 5.5 GHz. The port2's position along the x-axis is selected to be close to the shorting edge with minimum Q value (its y-axis position is determined by isolation, which will be introduced in Section III-D). When the best patch width and port2's position are selected, not only the impedance bandwidth of the $TM_{0.5,1}$ mode reaches the maximum, but also the Wi-Fi 6 higher band can be covered.

Thus, it has demonstrated that under the dimensions of 22.55 × 23.95 × 3 mm^3, when the maximum bandwidths of the half-mode patch are achieved, the Wi-Fi 6 bands are covered exactly at the same time. Based on the analysis above, the design guideline follows three steps. First, select proper patch size to make the first two modes resonate at 2.45 and 5.5 GHz using two ports. Second, optimize feeding positions so that both impedance trajectories in the Smith Chart have the minimum sizes. Third, use lumped components to make the two resonances with good matching condition. An iteration is required for the three steps.

B. Performance Comparison With Traditional Matching Method

To explain the superiority of the proposed matching method compared with the traditional matching method, the half-mode patch with the identical dimensions of the proposed is matched

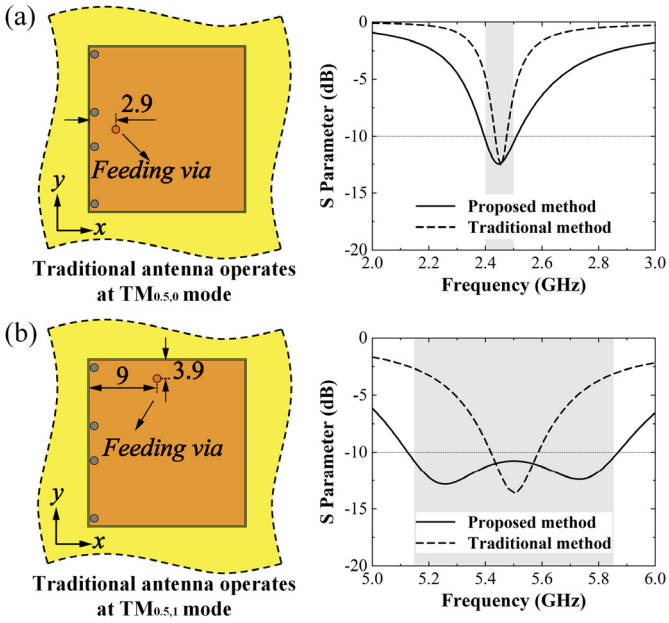

Fig. 7. Comparison of the proposed and traditional matching methods at (a) 2.45 GHz and (b) 5.5 GHz (unit: mm).

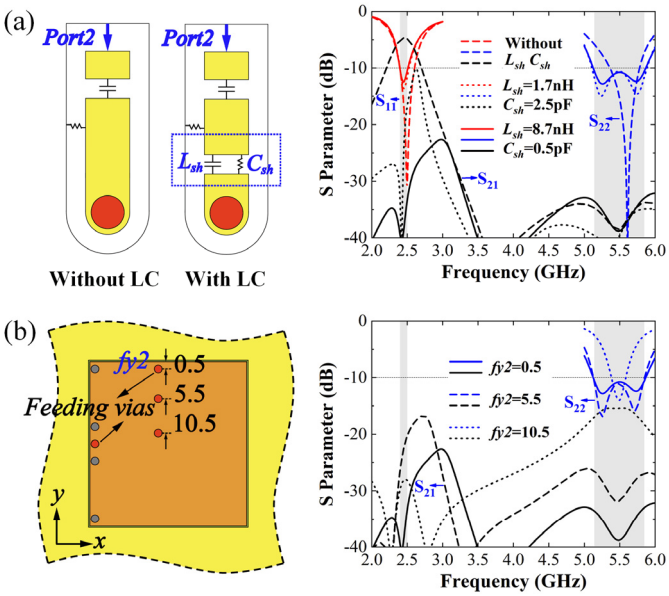

Fig. 8. Isolation consideration. Influences of (a) lumped filter and (b) port2's position (unit: mm).

by finding the natural 50-Ω impedance positions without using lumped components. For Wi-Fi 6 lower band, as shown in Fig. 7(a), when the feeding via locates 2.9 mm away from the shorting edge in the middle line, the natural resonance resonates at 2.45 GHz. The resultant bandwidth is only 40 MHz (2.44–2.48 GHz), which is worse than the proposed 100 MHz (2.4–2.5 GHz). For Wi-Fi 6 higher band, as shown in Fig. 7(b), when the feeding via locates 9 and 3.9 mm away from the shorting and upper edges, respectively, the natural resonance resonates at 5.5 GHz. The resultant bandwidth is 170 MHz (5.42–5.59 GHz), which is far worse than the proposed 700 MHz (5.15–5.85 GHz). In addition, the isolation is not considered yet. Therefore, the proposed matching method is superior to the traditional matching method.

C. Isolation Consideration

Isolation must be considered for antenna with multiple ports. Several factors that can improve the isolation level are introduced. Theoretically, the center plane of the half-mode patch is the electric node of the $TM_{0.5,1}$ mode. By placing the excitation ports of the $TM_{0.5,0}$ (port1) and $TM_{0.5,1}$ (port2) modes at and offset the center plane, respectively, port1 cannot excite the $TM_{0.5,1}$ mode, whereas port2 is able to excite the $TM_{0.5,0}$ mode. In other words, the power output from port2 cannot be absorbed by port1, whereas the power output from port1 can be absorbed by port2. Thus, as shown in Fig. 8(a), the isolation at a higher band is better than 33.4 dB, but at a lower band is as poor as 4.7 dB. To improve the isolation at the lower band, lumped filter composed by inductor and capacitor is loaded at port2 to prevent port2 from absorbing port1's power. When the filter composed by shunt 8.7-nH inductor and 0.5-pF capacitor is used, an isolation dip is produced at 2.45 GHz and the isolation is improved from 4.7 dB to better than 33.4 dB. The decoupling effect is determined by the Q factor of the filter: the larger the Q value (Q^2 is proportional to C_{sh}/L_{sh} for shunt LC), the narrower the frequency range of the isolation dip. As seen, when another filter composed by shunt 1.7 nH and 2.5 pF that is with a higher Q value is used (keep the product of $C_{sh} \times L_{sh}$ as constant), the isolation dip range decreases sharply, resulting in worse decoupling effect.

On the other hand, the port2's position affects isolation. Fig. 7(b) shows the influence of port2's y-axis position on isolation. When port2 gradually approaches to port1 ($fy2$ increases from 0.5 to 5.5 to 10.5 mm), the isolation level gets worse and worse: from 38.8 to 31.8 to 15.4 dB. Thus, port2 is placed near the upper/lower patch edge considering port decoupling.

IV. Conclusion

In this article, a small-volume dual-band half-mode patch antenna is proposed to address the exact coverage problem of the Wi-Fi 6 bands. The first two modes of the half-mode patch are engineered for Wi-Fi 6 dual-band coverage. The traditional matching and component matching methods are combined to improve the antenna performance. The proposed antenna is with three unique merits. First, it covers the Wi-Fi 6 bands in an exact way, indicating that the antenna space is taken up fully. Second, to the best of the authors' knowledge, the proposed antenna is with the smallest volume compared to all the reported Wi-Fi 6 dual-band patches. Third, the proposed antenna is with dual-port and aperture sharing properties, which suits the optimal Wi-Fi 6 RF front-end architecture. It shows a great potential for modern mobile terminals or IoT devices.

References

[1] Z. N. Chen, X. Qing, T. S. P. See, and W. K. Toh, "Antennas for WiFi connectivity," *Proc. IEEE*, vol. 100, no. 7, pp. 2322–2329, Jul. 2012.

[2] H. Xiaomu, S. Yan, and G. A. E. Vandenbosch, "Wearable button antenna for dual-band WLAN applications with combined on and off-body radiation patterns," *IEEE Trans. Antennas Propag.*, vol. 65, no. 3, pp. 1384–1387, Mar. 2017.

[3] R. B. V. B. Simorangkir, Y. Yang, L. Matekovits, and K. P. Esselle, "Dual-band dual-mode textile antenna on PDMS substrate for body-centric communications," *IEEE Antennas Wireless Propag. Lett.*, vol. 16, pp. 677–680, 2017.

[4] X. Zhang, L. Sun, Y. Li, and Z. Zhang, "A broadband dual-antenna pair based on half-open cavity with horizontally polarized radiation for Wi-Fi 6/6E application," *IEEE Trans. Antennas Propag.*, vol. 70, no. 6, pp. 4250–4258, Jun. 2022.

[5] W. Zhang, Y. Li, K. Wei, and Z. Zhang, "A two-port microstrip antenna with high isolation for Wi-Fi 6 and Wi-Fi 6E applications," *IEEE Trans. Antennas Propag.*, vol. 70, no. 7, pp. 5227–5234, Jul. 2022.

[6] S. Mirhadi, "Single-layer, dual-port, and dual-mode antenna with high isolation for WBAN communications," *IEEE Antennas Wireless Propag. Lett.*, vol. 21, no. 3, pp. 531–535, Mar. 2022.

[7] Y.-J. Lee, J.-H. Tarng, and S.-J. Chung, "A filtering diplexing antenna for dual-band operation with similar radiation patterns and low cross-polarization levels," *IEEE Antennas Wireless Propag. Lett.*, vol. 16, pp. 58–61, 2017.

[8] D. E. Brocker, Z. H. Jiang, M. D. Gregory, and D. H. Werner, "Miniaturized dual-band folded patch antenna with independent band control utilizing an interdigitated slot loading," *IEEE Trans. Antennas Propag.*, vol. 65, no. 1, pp. 380–384, Jan. 2017.

[9] X. Quan, R. Li, Y. Cui, and M. M. Tentzeris, "Analysis and design of a compact dual-band directional antenna," *IEEE Antennas Wireless Propag. Lett.*, vol. 11, pp. 547–550, 2012.

[10] Y. Zhang, Y. Zhang, D. Li, K. Liu, and Y. Fan, "Dual-polarized band-notched antenna without extra circuit for 2.4/5 GHz WLAN applications," *IEEE Access*, vol. 7, pp. 84890–84896, 2019.

[11] A. T. Mobashsher, M. T. Islam, and N. Misran, "A novel high-gain dual-band antenna for RFID reader applications," *IEEE Antennas Wireless Propag. Lett.*, vol. 9, pp. 653–656, 2010.

[12] L. Peng, C.-L. Ruan, and X.-H. Wu, "Design and operation of dual/triple-band asymmetric M-shaped microstrip patch antennas," *IEEE Antennas Wireless Propag. Lett.*, vol. 9, pp. 1069–1072, 2010.

[13] K.-L. Wong, C.-J. Chen, and W.-Y. Li, "Integrated four low-profile shorted patch dual-band WLAN MIMO antennas for mobile device applications," *IEEE Trans. Antennas Propag.*, vol. 69, no. 6, pp. 3566–3571, Jun. 2021.

[14] Z. Liang, J. Liu, Y. Li, and Y. Long, "A dual-frequency broadband design of coupled-fed stacked microstrip monopolar patch antenna for WLAN applications," *IEEE Antennas Wireless Propag. Lett.*, vol. 15, pp. 1289–1292, 2016.

[15] S. Liu, W. Wu, and D. Fang, "Single-feed dual-layer dual-band E-shaped and U-slot patch antenna for wireless communication application," *IEEE Antennas Wireless Propag. Lett.*, vol. 15, pp. 468–471, 2016.

[16] J. Tak, S. Woo, J. Kwon, and J. Choi, "Dual-band dual-mode patch antenna for on-/off-body WBAN communications," *IEEE Antennas Wireless Propag. Lett.*, vol. 15, pp. 348–351, 2016.

[17] N. Liu, L. Zhu, Z. Liu, and Y. Liu, "Dual-band single-layer microstrip patch antenna with enhanced bandwidth and beamwidth based on reshaped multiresonant modes," *IEEE Trans. Antennas Propag.*, vol. 67, no. 11, pp. 7127–7132, Nov. 2019.

[18] X. Y. Zhang, Y. Zhang, Y.-M. Pan, and W. Duan, "Low-profile dual-band filtering patch antenna and its application to LTE MIMO system," *IEEE Trans. Antennas Propag.*, vol. 65, no. 1, pp. 103–113, Jan. 2017.

[19] X. Liu, Y. Li, Z. Liang, S. Zheng, J. Liu, and Y. Long, "A method of designing a dual-band sector ring microstrip antenna and its application," *IEEE Trans. Antennas Propag.*, vol. 64, no. 11, pp. 4896–4901, Nov. 2016.

[20] L. Chang and H. Liu, "Low-profile and miniaturized dual-band microstrip patch antenna for 5G mobile terminals," *IEEE Trans. Antennas Propag.*, vol. 70, no. 3, pp. 2328–2333, Mar. 2022.

[21] S. Liu, S. Qi, W. Wu, and D. Fang, "Single-feed dual-band single/dual-beam U-slot antenna for wireless communication application," *IEEE Trans. Antennas Propag.*, vol. 63, no. 8, pp. 3759–3764, Aug. 2015.

[22] L. Chang, G. Zhang, and H. Wang, "Triple-band microstrip patch antenna and its four-antenna module based on half-mode patch for 5G 4×4 MIMO operation," *IEEE Trans. Antennas Propag.*, vol. 70, no. 1, pp. 67–74, Jan. 2022.

[23] S. Gao, L. Ge, D. Zhang, and W. Qin, "Low-profile dual-band stacked microstrip monopolar patch antenna for WLAN and car-to-car communications," *IEEE Access*, vol. 6, pp. 69575–69581, 2018.

[24] Z. G. Liu and Y. X. Guo, "Dual band low profile antenna for body centric communications," *IEEE Trans. Antennas Propag.*, vol. 61, no. 4, pp. 2282–2285, Apr. 2013.

[25] Y. Li, Z. Zhang, W. Chen, Z. Feng, and M. F. Iskander, "A switchable matching circuit for compact wideband antenna designs," *IEEE Trans. Antennas Propag.*, vol. 58, no. 11, pp. 3450–3457, Nov. 2010.

[26] H. Wang, Z. Zhang, Y. Li, and Z. Feng, "A dual-resonant shorted patch antenna for wearable application in 430 MHz band," *IEEE Trans. Antennas Propag.*, vol. 61, no. 12, pp. 6195–6200, Dec. 2013.

[27] L. Chang and H. Wang, "Dual-band four-antenna module covering N78/N79 based on PIFA for 5G terminals," *IEEE Antennas Wireless Propag. Lett.*, vol. 21, no. 1, pp. 168–172, Jan. 2022.

[28] L. Chang and H. Wang, "Miniaturized wideband four-antenna module based on dual-mode PIFA for 5G 4×4 MIMO applications," *IEEE Trans. Antennas Propag.*, vol. 69, no. 9, pp. 5297–5304, Sep. 2021.

[29] A. A. Salih and M. S. Sharawi, "A dual-band highly miniaturized patch antenna," *IEEE Antennas Wireless Propag. Lett.*, vol. 15, pp. 1783–1786, 2016.

Shan Gao (Student Member, IEEE) received the B.S. degree in electronics and information engineering from Xi'an Jiaotong University, Xi'an, China, in 2021, where she is currently pursuing the Ph.D. degree in electrical engineering.

Her current research interests include antenna design and theory, particularly in 5G mobile antennas and terminal antennas.

Le Chang (Senior Member, IEEE) received the B.S. degree in electronics and information engineering from Xidian University, Xi'an, China, in 2012, and the Ph.D. degree in electrical engineering from Tsinghua University, Beijing, China, in 2017.

In July 2017, he joined Huawei Technology Ltd., Beijing, as a Senior Antenna Engineer. Since 2021, he has been with Xi'an Jiaotong University, Xi'an, where he is currently an Associate Professor. He has authored or coauthored over 34 journal articles. His current research interests include 5G mobile antennas, millimeter-wave antennas, and beam scanning antennas.

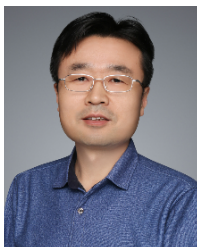

Anxue Zhang received the B.S. degree in electrical engineering from Henan Normal University, Xinxiang, Henan, China, in 1996, and the M.S. and Ph.D. degrees in electrical engineering from Xi'an Jiaotong University, Xi'an, China, in 1999 and 2003, respectively.

He is currently a Professor and the Director of the Institute of Electromagnetics and Information Technology, Xi'an Jiaotong University. He is also a member of the Academic Committee of the Key Laboratory of Ultra-High Speed Circuit Design and Electromagnetic Compatibility of the Ministry of Education. He has coauthored one book and more than 300 journal articles on these topics. His research interests include antenna and electromagnetic wave propagation, RF and microwave circuit design, and metamaterials.

Yue Li (Senior Member, IEEE) received the B.S. degree in telecommunication engineering from Zhejiang University, Hangzhou, Zhejiang, China, in 2007, and the Ph.D. degree in electronic engineering from Tsinghua University, Beijing, China, in 2012.

In June 2012, he was a Post-Doctoral Fellow with the Department of Electronic Engineering, Tsinghua University. In December 2013, he was a Research Scholar with the Department of Electrical and Systems Engineering, University of Pennsylvania, Philadelphia, PA, USA. He was also a Visiting Scholar with the Institute for Infocomm Research (I2R), A∗STAR, Singapore, in 2010, and the Hawaii Center of Advanced Communication (HCAC), University of Hawaii at Manoa, Honolulu, HI, USA, in 2012. Since January 2016, he has been with Tsinghua University, where he is currently an Assistant Professor. He is also an Associate Professor with the Department of Electronic Engineering, Tsinghua University. He has authored and coauthored over 90 journal articles and 45 international conference papers. He holds 15 granted Chinese patents. His current research interests include metamaterials, plasmonics, electromagnetics, nanocircuits, mobile and handset antennas, MIMO and diversity antennas, and millimeter-wave antennas and arrays.

Prof. Li was a recipient of the Issac Koga Gold Medal from the URSI General Assembly in 2017; the Second Prize of Science and Technology Award of the China Institute of Communications in 2017; the Young Scientist Awards from the conferences of ACES 2018, AT-RASC 2018, AP-RASC 2016, EMTS 2016, and URSI GASS 2014; the Best Paper Awards from the conferences of CSQRWC 2018, NCMMW 2018 and 2017, APCAP 2017, NCANT 2017, ISAPE 2016, and ICMMT 2016; the Outstanding Doctoral Dissertation of Beijing Municipality in 2013; and the Principal Scholarship of Tsinghua University in 2011. He is serving as an Associate Editor for IEEE TRANSACTIONS ON ANTENNAS AND PROPAGATION, IEEE ANTENNAS AND WIRELESS PROPAGATION LETTERS, and *Computer Applications in Engineering Education* and on the Editorial Board of *Scientific Report*.

Zhijun Zhang (Fellow, IEEE) received the B.S. and M.S. degrees from the University of Electronic Science and Technology of China, Chengdu, China, in 1992 and 1995, respectively, and the Ph.D. degree from Tsinghua University, Beijing, China, in 1999.

In 1999, he was a Post-Doctoral Fellow with the Department of Electrical Engineering, University of Utah, Salt Lake City, UT, USA, where he was appointed as a Research Assistant Professor in 2001. In May 2002, he was an Assistant Researcher with the University of Hawaii at Manoa, Honolulu, HI, USA. In November 2002, he joined Amphenol T&M Antennas, Vernon Hills, IL, USA, as a Senior Staff Antenna Development Engineer, where he was then promoted to the position of Antenna Engineer Manager. In 2004, he joined Nokia Inc., San Diego, CA, USA, as a Senior Antenna Design Engineer. In 2006, he joined Apple Inc., Cupertino, CA, USA, as a Senior Antenna Design Engineer, where he was then promoted to the position of Principal Antenna Engineer. Since August 2007, he has been with Tsinghua University, where he is currently a Professor with the Department of Electronic Engineering.

Prof. Zhang is the author of *Antenna Design for Mobile Devices* (Wiley, first edition 2011, second edition 2017). He served as an Associate Editor for the IEEE TRANSACTIONS ON ANTENNAS AND PROPAGATION from 2010 to 2014 and the IEEE ANTENNAS AND WIRELESS PROPAGATION LETTERS from 2009 to 2015.